Distributed Coordinated Motion Tracking of the Linear Switched Reluctance Machine-Based Group Control System

Bo Zhang, *Member, IEEE*, Jianping Yuan, Li Qiu, Norbert Cheung, *Senior Member, IEEE*, and J. F. Pan, *Member, IEEE*

***Abstract*—The coordinated tracking control for the group motion control system based on three direct-drive double-sided linear switched reluctance motors (LSRMs) is investigated in this paper. The system construction for the proposed coordinated tracking system is elaborated, including the unit system and group system design, communication configuration among unit systems, and stability and performance analysis of the group system. The coordinated control performance is concentrated on three identical LSRMs with different communication topologies. Experimental results demonstrate that necessary bidirectional interactions between the unit systems contribute to the coordination performance. The maximum dynamic tracking error within $\pm$0.4 mm can be achieved under the sinusoidal reference of 30-mm amplitude and 0.2-Hz frequency.**

***Index Terms*—Coordinated tracking, group motion control system, linear switched reluctance motor (LSRM).**

I. Introduction

LINEAR translation, as one of the most common forms of motion in the industry, can be found extensively in parts assembly, chip manufacture, printed circuit board drilling areas, etc. With the fast paces of smart and highly integrated control chips, the development of intelligent coordinated operating linear motion control systems with the capability of batch processing, fast speed, and high precision becomes available. For example, an assembly gantry system with three degrees of freedom has two or more working units. The traditional processing procedure is that all working units operate in sequence. That is, the second unit is often unable to process until the first one has finished its job. If some of the working units are able to actuate according to the others' information, such as speed, position, etc., the units may operate simultaneously and coordinately to accomplish one assembly task, and the overall motion control system can achieve a better performance such as the annihilation of accumulated errors with improved efficiency.

To realize a coordinated operation, each working unit can be connected to the main controller by wired or wireless means to transmit its real-time working status to the others. The main controller is responsible for the control decision of operation from all units, receiving and dispatching all required information for them at the same time. However, the "centralized coordination" manner requires the main controller to possess a fast computing and data processing capability, and it requires the collection and exchange of information globally [1]. The entire system collapses as the main controller fails. If system fault occurs, such as signal transmission failure or disconnection from one or more units, the whole control system is bound to yield performance deterioration or even malfunction [2]. In addition, for a group motion control system with numerous or spatially dispersed linear machines, the centralized control mode will be too expensive to be implemented, and even if they could be done, the resulting system is not robust or efficient [3].

Apart from the centralized mode, the distributed or decentralized operation does not require any central processing controllers. Any working unit can be considered as an autonomous "multiagent," and each unit system has its own controller, transducer, etc., which individually conforms to a typical closed-loop linear motion control system [4]. The ultimate global control goal can be emerged only by local communications among the independent unit closed-loop systems with local controllers, without requiring global supervision or decision [5]. For example, many closed-loop systems based on linear machines can communicate with each other through local controllers, and all machines can work cooperatively to achieve one ultimate task such as chassis welding for automobiles.

As the actuator of the linear motion control system, a direct-drive translational machine has the advantages of a simplified mechanical structure, high reliability, and reduced mechanical adjustments or maintenance [6]. Among the linear machines,

Manuscript received April 28, 2015; revised June 17, 2015 and August 20, 2015; accepted September 22, 2015. Date of publication October 26, 2015; date of current version February 8, 2016. This work was supported in part by the National Natural Science Foundation of China under Grants 51477103, 51577121, 11572248, and 61403258, in part by the Guangdong Natural Science Foundation under Grants S2014A030313564 and S2015A010106017, and in part by the Shenzhen Government under Codes JCYJ20130329144017199 and JCYJ 20140418182819153.

B. Zhang is with the Shenzhen Key Laboratory of Electromagnetic Control, College of Mechatronics and Control Engineering, Shenzhen University, Shenzhen 518060, China, and also with the National Key Laboratory of Aerospace Flight Dynamics, Northwestern Polytechnical University, Xi'an 710072, China.

J. Yuan is with the National Key Laboratory of Aerospace Flight Dynamics, Northwestern Polytechnical University, Xi'an 7100072, China.

L. Qiu and J. F. Pan are with the Shenzhen Key Laboratory of Electromagnetic Control, College of Mechatronics and Control Engineering, Shenzhen University, Shenzhen 518060, China (e-mail: pan_jian_fei@163.com).

N. C. Cheung is with the Department of Electrical Engineering, Hong Kong Polytechnic University, Kowloon, Hong Kong.

Color versions of one or more of the figures in this paper are available online at http://ieeexplore.ieee.org.

Digital Object Identifier 10.1109/TIE.2015.2494844

a linear switched reluctance motor (LSRM) owns a robust and stable mechanical structure. It is more suitable for mass production and the implementation of a distributed linear motion control system due to its simple construction and low cost [7]. Current research mainly focuses on the performance improvement for the single-LSRM-based control applications [8]–[10]. In [8], a passivity-based control algorithm is proposed for a position tracking system of the LSRM to overcome the inherent nonlinear characteristics and render system robustness against uncertainties and bounded disturbances. An adaptive controller is proposed to combat the difficulties and uncertain control behaviors of a double-sided LSRM in [9]. A nonlinear proportional differential (PD) controller based on the tracking differentiator is introduced for the LSRM-based real-time suspension system to achieve a better dynamic response [10].

The study of a linear machine-based distributed coordinated group motion control system has yet to be reported. The cooperative control theory of dynamic systems based on the decentralized manner provides a theoretical support for the coordinated tracking of the multiple-LSRM-based group motion control system. Previous studies on decision-making mechanism in particle groups, such as flocking [11], swarming [12], and schooling [13], provide a useful insight for the coordinated control of LSRMs. The consensus algorithms for second-order dynamics have been recently researched by Ren and Beard [14]. The extensional algorithms for the unit of a general linear system are further discussed by Qu *et al.* [15]. The coordinated and cooperative control scheme based on the consensus algorithm has been successfully applied to the formation control of multiple vehicles [15] and flight vehicles [16]. In rendezvous problems, the consensus algorithm is applied for all units in a group to assemble at a certain location simultaneously [17]. Other applications include multi-spacecraft attitude synchronization and tracking [18]–[20], sensor network decision making [21], and robot synchronization [22]. Unfortunately, the majority of the research work discussed earlier is only focused on theoretical analysis or mathematical simulation, based solely on ideal assumptions such as synchronous time sampling, unrestricted communication bandwidth, perfect information transmission, etc.

The contribution of this paper includes the following. First, the coordinated tracking in a decentralized manner has been first attempted for group motion control systems based on three independent direct-drive asymmetric double-sided LSRMs [23]. Second, the construction of the coordinated tracking system, including communication configuration, controller design, etc., is further clarified, together with stability and performance analysis. Third, four different communication topologies are studied for the proposed group tracking control system, and the control performance from each topology is analyzed.

II. Background Theory

A. Mathematical Model of the LSRM Unit System

Any one phase of the LSRM from the ith unit system can be described in the voltage balancing equation as [10]

$$u_{i_k} = R_{i_k} i_{i_k} + \frac{d\lambda_{i_k}}{dt}, \quad k = a, b, c \tag{1}$$

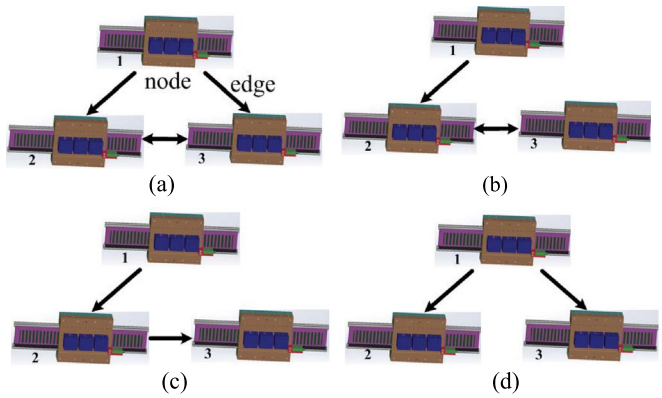

Fig. 1. Communication topology graphs.

where u_{i_k}, R_{i_k}, and i_{i_k} are the terminal voltage, coil resistance, and current, respectively. λ_{i_k} represents the flux linkage for the kth winding. Rearranging (1) by neglecting the mutual and leakage flux linkage, we have

$$\frac{di_{i_k}}{dt} = \frac{u_{i_k} - R_{i_k} i_{i_k} - \frac{\partial \lambda(i_{i_k}, x_i)}{\partial x_i} \cdot \frac{dx_i}{dt}}{\frac{\partial \lambda(i_{i_k}, x_i)}{\partial i_{i_k}}}. \tag{2}$$

The mechanical representations that depict the entire motion behavior for any unit control system can be characterized as [9]

$$\frac{dx_i}{dt} = v_i \tag{3}$$

$$\frac{dv_i}{dt} = \frac{(f_i^* - B_i v_i - fl_i)}{m_i} \tag{4}$$

where x_i, v_i, B_i, m_i, f_i^*, and fl_i represent the position, velocity, friction coefficient, mass, and electromagnetic and load forces for the ith LSRM, respectively. Equations (3) and (4) can be further expressed as

$$m_i \cdot \frac{d^2 x_i}{dt^2} + B_i \cdot \frac{dx_i}{dt} + fl_i = f_i^* \tag{5}$$

f_i^* can be expressed as

$$f^*(i_{i_k}, x_i) = \frac{\partial W'(i_{i_k}, x_i)}{\partial x_i} \tag{6}$$

where $W'(i_{i_k}, x_i)$ denotes the coenergy.

B. Graph Theory and Communication Topology

In general, the information exchange among LSRM-based group motion control systems can be modeled by a graph G consisting of a nonempty finite set of nodes $V = \{v_1, \ldots, v_N\}$ and an edge set $E \subseteq V \times V$ [24]. The node v_i denotes the ith LSRM-based unit system. An edge $e_{ij} \in E$ denotes that there is a directed information propagative flow from the jth to the ith unit system. A neighbor set of the ith unit system is symbolized as $N_i = \{v_j \in V : e_{ij} \in E\}$. For example, the neighbors of unit system 2 are systems 1 and 3 in Fig. 1(a). A path from node v_i to v_j is a sequence of successive edges in E that connects

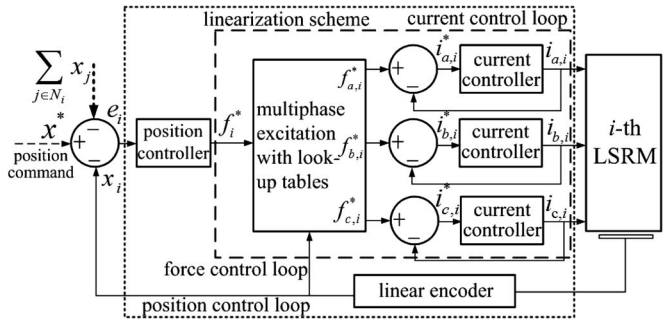

Fig. 2. Position control diagram for ith unit system.

node v_j to node v_i. A directed graph G has a spanning tree if G has a node to which there exists a path form every other node [25]. For the LSRM-based unit systems, as shown in Fig. 1, the edges of the directed graph can be represented by the directed lines and arrows. For all the cases from Fig. 1(a)–(d), there exist spanning trees, and the root node is system 1.

The adjacency matrix $\boldsymbol{A} = [a_{ij}] \in R^{N\times N}$ associated with graph G is defined by $a_{ij} > 0$ if $e_{ij} \in E$; otherwise, $a_{ij} = 0$, and $a_{ii} = 0$ for all $i = 1, \ldots, N$. Without considering weights, $a_{ij} = 1$ if $e_{ij} \in E$. The Laplacian matrix $\boldsymbol{L} = [l_{ij}] \in R^{N\times N}$ is defined as $l_{ii} = \sum_{i\neq j} a_{ij}$, and $l_{ij} = -a_{ij}$ for $i \neq j$.

C. Coordinated Control of LSRM-Based Group System

The aforementioned graph G represents the communication topology of the information flow among unit systems, and the topology restricts the allowed communications between the nodes. In addition, the communication topology can be artificially modified for the group system as necessary. Therefore, the ultimate goal of coordinated control for the group system is to realize position or velocity synchronization for all unit systems based on G.

The control law for each LSRM unit system is given by $u_i = k_i(x_i, x_j)$, $\{x_j | j \in N_i\}$, which relies on the position and velocity information from itself and its neighbors in N_i, i.e., the output of each node depends on the specified subset of all the nodes, of which states can be received by node i. Therefore, the coordination of the group system can be essentially considered as a consensus problem provided that $u_i(t)$, $i = 1, \ldots, N$, $\lim_{t\to\infty} \|\boldsymbol{x}_i - \boldsymbol{x}_j\| = 0$ with $\boldsymbol{x}_{i,j} = [x_{i,j}, \dot{x}_{i,j}]^T$, which represents that the states from each unit system can achieve the global control goal for any initial states of $i, j = 1, \ldots, N$ [26].

III. Controller Design

A. Position Controller for the Unit Systems

For each unit system, the typical dual-loop control scheme is employed, and the outer position controller with the PD algorithm is applied with the control diagram illustrated in Fig. 2 in the time domain. The operation of the outer position control loop is based on the assumption that the current controllers have a perfect tracking capability. Since an LSRM commonly characterizes a highly nonlinear relationship, the linearization scheme of the multiphase excitation combined with 2-D 27 × 27-matrix lookup tables is applied to combat the nonlinearities between force with respect to current and position for each phase [27]. The multiphase excitation of the force control loop calculates the phase force command $f^*_{k,i}$ $(k = a, b, c)$ from the total force command f^*_i derived from the position controller [27]. $\sum_{j\in N_i} x_j$ represents the set of the neighbors' position information, and e_i stands for the error sum from x_j to x_i or the error sum from x_j to x_i plus $x^* - x_i$.

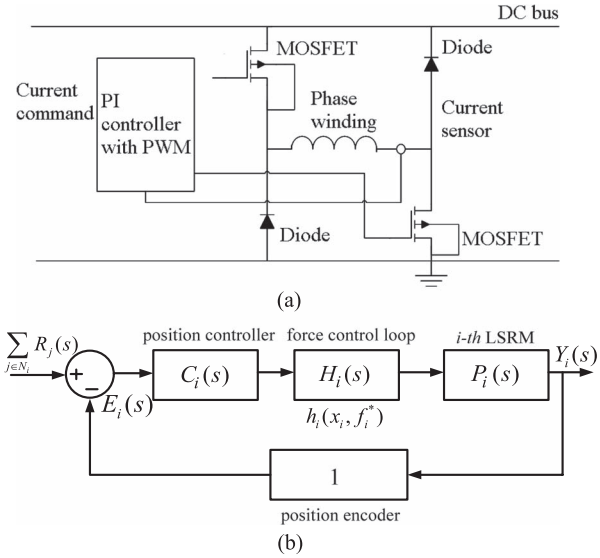

Fig. 3. (a) Converter topology and (b) block diagram for the ith unit system.

The PD position controller takes the form

$$C_i(s) = K_{p,i} + K_{d,i}s \tag{7}$$

where $K_{p,i}$ and $K_{d,i}$ are the proportional and differential gains for the ith unit system, respectively. The whole force control loop can be represented as a nonlinear function $h_i(x_i, f^*_i) > 0$ with respect to position and total force command, and $H_i(s)$ is the Laplace transform of $h_i(x_i, f^*_i) > 0$ after linearization [28].

For the current controller for either axes, three asymmetric bridge pulse width modulation (PWM) converters are employed so that each phase can be controlled independently. Fig. 3(a) shows the circuit of the converter for one axis [9]. According to the control block diagram in the complex domain from Fig. 3(b), the closed-loop transfer function between position reference $R_i(s)$ and feedback $Y_i(s)$, neglecting load force, can thus be represented by

$$\begin{aligned} H'_i(s) &= \frac{Y_i(s)}{R_i(s)} \\ &= \frac{(K_{p,i} + K_{d,i}s)\cdot H_i(s)\cdot \frac{K_{s,i}}{m_i s^2 + B_i s}}{1 + (K_{p,i} + K_{d,i}s)\cdot H_i(s)\cdot \frac{K_{s,i}}{m_i s^2 + B_i s}} \\ &= \frac{K_{s,i}\cdot H_i \cdot (K_{p,i} + K_{d,i}s)}{m_i s^2 + (B_i + K_{d,i}K_{s,i}H_i)s + K_{p,i}K_{s,i}H_i} \end{aligned} \tag{8}$$

where $K_{s,i}$ is the system gain. $\sum_{j\in N_i} R_j(s)$ is the Laplace transform of $\sum_{j\in N_i} x_j$. For the current controller for either axes, three asymmetric bridge PWM converters are employed

so that high dynamic response can be enjoyed independently in each motor phase. The following figure shows the circuit of the converter for one axis.

B. Coordinated Control Design

Rearranging (5) in the state-space form, we have

$$\begin{bmatrix}\dot{x}_i\\ \ddot{x}_i\end{bmatrix}=\begin{bmatrix}0 & 1\\ 0 & -\frac{B_i}{m_i}\end{bmatrix}\begin{bmatrix}x_i\\ \dot{x}_i\end{bmatrix}+\begin{bmatrix}0\\ \frac{1}{m_i}\end{bmatrix}u_i \tag{9}$$

where $u_i = f_i^* - fl_i$.

The consensus algorithm for the general second-order linear system is applied to design the coordinated control law [29] for the proposed group motion control system. It is formulated as

$$u_i=-c\sum_{j=1}^{N}a_{ij}[K_{p,i}(x_j(t)-x_i(t))+K_{d,i}(\dot{x}_j(t)-\dot{x}_i(t))] \tag{10}$$

where c is the coupled scalar feedback gain and a_{ij} is the entry of adjacency matrix $\boldsymbol{A}$ associated with graph G. The velocity feedback terms ($\dot{x}_i(t)$ and $\dot{x}_j(t)$) are obtained by the differential of position ($x_i(t)$ and $x_j(t)$) from the position control loop. The dynamic equation for the ith LSRM unit system can thus be represented as

$$\begin{bmatrix}\dot{x}_i\\ \ddot{x}_i\end{bmatrix}=\begin{bmatrix}0 & 1\\ 0 & -\frac{B_i}{m_i}\end{bmatrix}\begin{bmatrix}x_i\\ \dot{x}_i\end{bmatrix}-c\sum_{j=1}^{N}a_{ij}\begin{bmatrix}0\\ \frac{1}{m_i}\end{bmatrix}[K_{p,i}\ \ K_{d,i}]\begin{bmatrix}x_j(t)-x_i(t)\\ \dot{x}_j(t)-\dot{x}_i(t)\end{bmatrix}. \tag{11}$$

The dynamic equation for the multiple-LSRM unit system can thus be derived as

$$\begin{bmatrix}\dot{x}_1\\ \ddot{x}_1\\ \vdots\\ \dot{x}_N\\ \ddot{x}_N\end{bmatrix}=\left\{\boldsymbol{I}_N\otimes\begin{bmatrix}0 & 1\\ 0 & -\frac{B_i}{m_i}\end{bmatrix}-c\boldsymbol{L}\otimes\begin{bmatrix}0\\ \frac{1}{m_i}\end{bmatrix}[K_{p,i}\ \ K_{d,i}]\right\}\begin{bmatrix}x_1\\ \dot{x}_1\\ \vdots\\ x_N\\ \dot{x}_N\end{bmatrix} \tag{12}$$

where $\boldsymbol{I}_N$ is the Nth identity matrix and $\boldsymbol{L}$ is the Laplacian matrix. Let

$$\begin{aligned}\boldsymbol{x}&=[x_1,\dot{x}_1,\ldots,x_N,\dot{x}_N]^T\\ \boldsymbol{A}_i&=\begin{bmatrix}0 & 1\\ 0 & -\frac{B_i}{m_i}\end{bmatrix}\\ \boldsymbol{B}_i&=\begin{bmatrix}0\\ \frac{1}{m_i}\end{bmatrix}\\ \boldsymbol{K}_i&=[K_{p,i}\ \ K_{d,i}].\end{aligned}$$

Since all the LSRM unit systems are identical, the subscripts for $\boldsymbol{A}_i, \boldsymbol{B}_i, \boldsymbol{K}_i$ can be neglected. Therefore, the above equation is represented as

$$\dot{\boldsymbol{x}}=(\boldsymbol{I}_N\otimes\boldsymbol{A}-c\boldsymbol{L}\otimes\boldsymbol{BK})\boldsymbol{x}. \tag{13}$$

C. Stability Analysis

To analyze the stability for the LSRM unit system as represented in (11) and the group system in (13), the following lemma is employed to prove **Theorem 1**.

Lemma 1: When graph G contains a spanning tree, the eigenvalues of the Laplacian matrix $\boldsymbol{L}(G)$ can be satisfied as $\lambda_1 = 0$, and $\mathrm{Re}(\lambda_i) > 0, i = 2,\ldots,N$ [14].

Theorem 1: Group system (13) is asymptotically stable if and only if all the matrices

$$\boldsymbol{A} \text{ and } \boldsymbol{A}-c\lambda_i\boldsymbol{BK},\quad i=2,\ldots,N \tag{14}$$

are Hurwitz.

Proof: When directed graph G contains a spanning tree, the nonsingular matrix $\boldsymbol{M}$ can be obtained such that the Jordan form $\boldsymbol{J}$ of the Laplacian matrix of G can be calculated by $\boldsymbol{L}(G)=\boldsymbol{M}^{-1}\boldsymbol{JM}$. According to **Lemma 1**, the form of $\boldsymbol{J}$ satisfies

$$\boldsymbol{J}=\begin{bmatrix}0 & 0 & \ldots & 0\\ 0 & \boldsymbol{J}(\lambda_2) & \ldots & 0\\ \vdots & \vdots & \ddots & \vdots\\ 0 & 0 & \ldots & \boldsymbol{J}(\lambda_N)\end{bmatrix}. \tag{15}$$

$\boldsymbol{J}(\lambda_i)$ are the Jordan blocks associated with λ_i, $i = 2,\ldots,N$. The similarity transformation of the matrix $\boldsymbol{I}_N\otimes\boldsymbol{A}-c\boldsymbol{L}\otimes\boldsymbol{BK}$ is a block triangular matrix as

$$\begin{aligned}&(\boldsymbol{M}^{-1}\otimes\boldsymbol{I}_m)(\boldsymbol{I}_N\otimes\boldsymbol{A}-c\boldsymbol{L}\otimes\boldsymbol{BK})(\boldsymbol{M}\otimes\boldsymbol{I}_m)\\ &\qquad=(\boldsymbol{I}_N\otimes\boldsymbol{A}-c\boldsymbol{J}\otimes\boldsymbol{BK}).\end{aligned} \tag{16}$$

The above deduction indicates that the group system matrix $\boldsymbol{I}_N\otimes\boldsymbol{A}-c\boldsymbol{L}\otimes\boldsymbol{BK}$ is equivalent to the following:

$$\mathrm{diag}\{\boldsymbol{A},\boldsymbol{A}-c\lambda_2\boldsymbol{BK},\ldots,\boldsymbol{A}-c\lambda_N\boldsymbol{BK}\}. \tag{17}$$

Since a state-space transformation does not change the eigenvalues, $\boldsymbol{I}_N\otimes\boldsymbol{A}-c\boldsymbol{J}\otimes\boldsymbol{BK}$ is Hurwitz if and only if $\boldsymbol{A}-c\lambda_i\boldsymbol{BK}$, $i=2,\ldots,N$ and $\boldsymbol{A}$ are Hurwitz. Similarly, the asymptotical stability of system (13) can be guaranteed. This proves **Theorem 1**. ■

By **Lemma 1**, on the premise that all unit systems in accordance to the matrix pair $(\boldsymbol{A}, \boldsymbol{B})$ are stabilizable, if the graph has a spanning tree with the leader as the root node, system (13) can be guaranteed to be stable with a proper selection of both c and $\boldsymbol{K}$ to satisfy condition (14). In addition, the selection of both c and $\boldsymbol{K}$ must conform to a specified graph topology. Simultaneously, **Theorem 1** also implies that a control law $\boldsymbol{K}$ stabilizing the single LSRM may fail to stabilize the group system (13). The method of determining c and $\boldsymbol{K}$ is provided in [26].

Remark of Scope of Stability: From the aforementioned deduction, on the premise that 1) there is a spanning tree [14] in graph G and 2) if and only if $\boldsymbol{A}$ and $\boldsymbol{A}-c\lambda_i\boldsymbol{BK}, i=2,\ldots,N$ is Hurwitz stable, i.e., the real parts of the eigenvalues of $\boldsymbol{A}$ and $\boldsymbol{A}+c\lambda_i\boldsymbol{BK}$ are strictly negative (λ_i, $i=2,\ldots,N$ represents the nonzero eigenvalues of Laplacian matrix $\boldsymbol{L}$ of G), then the

group system (13) is stable. $\boldsymbol{I}_m$ is the mth identity matrix, and m stands for the dimension of the system states from an LSRM.

D. Performance Analysis

For analyzing the converging speed of the group system (13), the following lemma is introduced.

Lemma 2: Let $\lambda_i, i = 1, \ldots, N, \mu_j$ and $\gamma_j, j = 1, \ldots, m$ be the eigenvalues of $\boldsymbol{L}$, $\boldsymbol{BK}$ and $\boldsymbol{A}$, respectively, corresponding to the eigenvectors $\nu_i, i = 1, \ldots, N, \upsilon_j$ and $\vartheta_j, j = 1, \ldots, m$. Then, $\eta_k = \gamma_j - c\lambda_i\mu_j,\ k = 1, \ldots, mN$ are the eigenvalues associated with the eigenvectors $\varphi_k = \nu_i \otimes \upsilon_j\vartheta_j$ of the state matrix of the group system (13).

Proof: 1) According to the property of the Kronecker product, $\gamma_j \cdot \mathbf{1}_N$ and $\lambda_i \cdot \mu_j$ are the eigenvalues of $\boldsymbol{I}_N \otimes \boldsymbol{A}$, $\boldsymbol{L} \otimes \boldsymbol{BK}$, respectively. Obviously, $\gamma_j - c\lambda_i\mu_j,\ i = 1, \ldots, N, j = 1, \ldots, m$ are the eigenvalues of the group system (13) in accordance with the property of the square matrix. 2) Let $\nu_i \otimes \upsilon_j\vartheta_j$ be multiplied by the state matrix of (13), and the following derivation can be given as:

$$\begin{aligned}
&(\boldsymbol{I}_N \otimes \boldsymbol{A} - c\boldsymbol{L} \otimes \boldsymbol{BK})(\nu_i \otimes \upsilon_j\vartheta_j) \\
&\quad = (\boldsymbol{I}_N \otimes \boldsymbol{A})(\nu_i \otimes \upsilon_j\vartheta_j) - (c\boldsymbol{L} \otimes \boldsymbol{BK})(\nu_i \otimes \upsilon_j\vartheta_j) \\
&\quad = \boldsymbol{I}_N\nu_i \otimes \boldsymbol{A}\vartheta_j\upsilon_j - c\boldsymbol{L}\nu_i \otimes \boldsymbol{BK}(\upsilon_j\vartheta_j) \\
&\quad = \nu_i \otimes \gamma_j\vartheta_j\upsilon_j - c\lambda_i\nu_i \otimes \mu_j\upsilon_j\vartheta_j \\
&\quad = (\gamma_j - c\lambda_i\mu_j)(\nu_i \otimes \upsilon_j\vartheta_j). \qquad (18)
\end{aligned}$$

Lemma 2 is proved. ■

Let $\boldsymbol{\Phi} = [\varphi_1\ \varphi_2\ \cdots\ \varphi_{mN}]$ be the matrix consisting of the normalized eigenvectors $\varphi_k = \nu_i \otimes \upsilon_j\vartheta_j$ of $\boldsymbol{I}_N \otimes \boldsymbol{A} - c\boldsymbol{L} \otimes \boldsymbol{BK}$, corresponding to its eigenvalues $\eta_k = \gamma_j - c\lambda_i\mu_j,\ k = 1, \ldots, mN$. The solution of the group system (13), initialized from $\boldsymbol{x}(0)$, can be given in accordance with **Lemma 1** and **Lemma 2** from the following:

$$\begin{aligned}
\boldsymbol{x}(t) &= e^{(\boldsymbol{I}_N \otimes \boldsymbol{A} - c\boldsymbol{L} \otimes \boldsymbol{BK})t}\boldsymbol{x}(0) \\
&= e^{\boldsymbol{\Phi\Lambda\Phi}^{-1}t}\boldsymbol{x}(0) \\
&= \boldsymbol{\Phi}e^{\boldsymbol{\Lambda}t}\boldsymbol{\Phi}^{-1}\boldsymbol{x}(0) \\
&= \boldsymbol{\Phi}\begin{bmatrix} e^{\boldsymbol{\Lambda}(\gamma_j)t} & 0 & \cdots & 0 \\ 0 & e^{\boldsymbol{\Lambda}(\gamma_j - c\lambda_2\mu_j)t} & \cdots & 0 \\ \vdots & \vdots & \ddots & \vdots \\ 0 & 0 & 0 & e^{\boldsymbol{\Lambda}(\gamma_j - c\lambda_N\mu_j)t} \end{bmatrix}\boldsymbol{\Phi}^{-1}\boldsymbol{x}(0). \qquad (19)
\end{aligned}$$

We can distinctly discern that the eigenvalue which has the minimum absolute value of the real part decides the converging speed of system (13) under the premise that the real parts of all eigenvalues $\gamma_j - c\lambda_i\mu_j$ are negative. Since the first eigenvalue of $\boldsymbol{L}$ satisfies $\lambda_1 = 0$, $\min(|\mathrm{Re}(\gamma_j - c\lambda_i\mu_j)|)$ is equivalent to $\min(|\mathrm{Re}(\gamma_j)|)$.

Therefore, we can obtain the conclusion that the state matrix $\boldsymbol{A}$ of the LSRM determines the converging speed of the group system (13). In addition, the bigger the value of $\min(|\mathrm{Re}(\gamma_j)|)$, the faster the converging speed that the system (13) possesses.

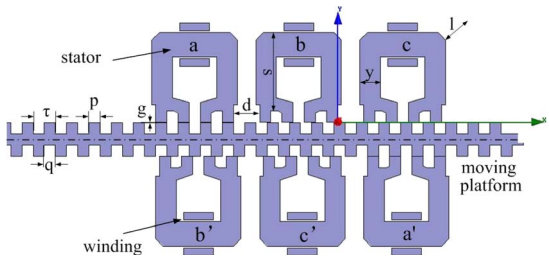

Fig. 4. (a) LSRM structure (to correspond a, b, c representation of phase), (b) unit control system, and (c) control structure of the group system .

IV. System Construction

The control objects are three identical LSRMs that conform to the "6/4" switched reluctance machine structure. A double-sided machine arrangement guarantees a more stable and reliable output performance [9], and the asymmetry of the stators ensures a higher force-to-volume ratio [23], as shown in Fig. 4(a). The stator base comprises six stators with windings, and each phase is magnetically decoupled. The silicon-steel plates are stacked and fixed into the moving platform, and a pair of linear guides is employed to facilitate the linear motion of the moving platform. A linear magnetic encoder with the

TABLE I
MAJOR SPECIFICATIONS

Symbol	Quantity	Value
M	Mass of moving platform	3.8 kg
M'	Mass of stator	5.0 kg
P	Pole width	6 mm
τ	Pole pitch	12 mm
R	Phase resistance	2 ohm
g	Air gap length	0.3 mm
N	Number of turns	200
l	Stack length	50 mm

TABLE II
CONTROLLER GAINS

Symbol	Quantity	Value
$K_{p,i}$	Proportion gain	10
$K_{d,i}$	Differential gain	0.25
c	Coupled gain	1

resolution of 1 μm is mounted onto the stator base for real-time position information collection. Table I demonstrates the major specifications of the machine.

The controllers are three dSPACE1104 control boards with onboard 250-MHz floating-point processors. Each control platform consists of two 24-b incremental encoder channels and six channels of 12-b analog input and output, respectively. The serial port interface is employed for the communication between the LSRM unit systems. The control card can directly interface with Real-Time Workshop and MATLAB/SIMULINK, and control parameters can be modified online.

Each closed-loop unit position control system mainly includes the LSRM, the power supply with transformers, and the dSPACE interface, as shown in Fig. 4(b). For each unit system, the sampling rate for the outer position control is 0.25 kHz, and the current loop is regulated by three commercial amplifiers that are capable of inner current control with a 20-kHz switching frequency based on the proportion integral algorithm. The switching frequency from the inner current loop is fast enough for position loop regulation after the current regulation has been completely settled.

Communication between unit systems is realized by the serial port with RS232 protocol. The baud rate is 57 600 with the data and stop bit set as 8 and 1, respectively. According to Fig. 1 of the communication topology of the three unit systems, the overall control structure of the group system can be represented as shown in Fig. 4(c). "External signals" represent the neighbors' position information and also the reference signal for unit system 1. "Internal signals" are the position information within the unit systems.

V. EXPERIMENTAL RESULTS

Table II tabulates the proportion and differential gains according to the constraints depicted in [26]. It can be verified by the stability analysis that all the parameters from Table II fall into the scope of stability for all of the aforementioned graph topologies depicted in Fig. 1. The proportional and differential

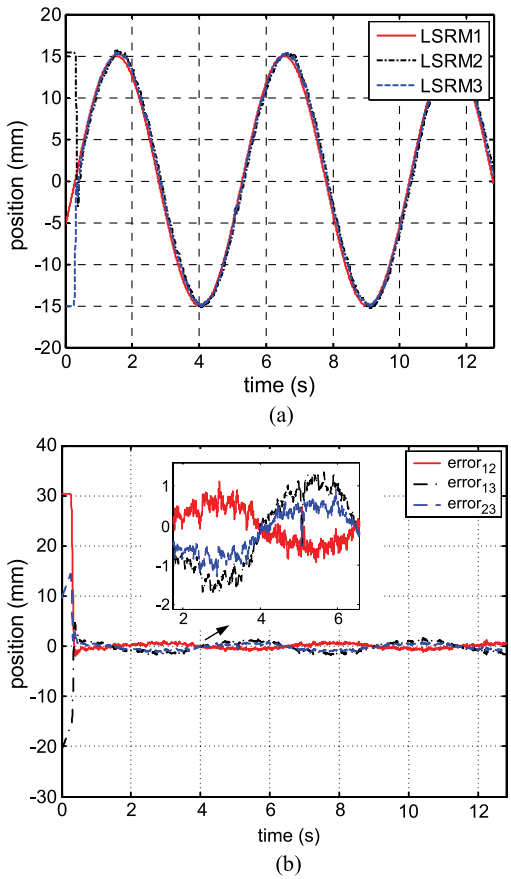

Fig. 5. Dynamic response of (a) position and (b) error of graph ①.

gains are the same for all LSRMs, and the gains are regulated based on trial and error experimentally [27].

The graphs are denoted by ①–④, respectively. To fully inspect the dynamic responses from the different topologies, the position reference signal is set as the sinusoidal waveform with an amplitude of 30 mm and a frequency of 0.2 Hz. The reference signal is generated by an external signal generator, and it is collected by the analog-to-digital channel of the control platform of unit system 1. After unit system 1 enters the steady state, the coordination control algorithm starts at 0.25 s. According to graphs ①–④, unit system 1 is the root node of the communication topology. It is clear that unit system 1 is strongly led by the reference signal, and its performance is not affected by unit system 2 or 3. Therefore, the tracking of unit system 1 is similar to a single-LSRM control problem, and unit system 1 also acts as an interface to the external reference signal for the entire group system.

Figs. 5(a)–8(a) illustrate the dynamic tracking profiles from graphs ①–④, and Figs. 5(b)–8(b) are the dynamic error response waveforms, respectively. In graph ①, the dynamic error profiles from the reference of the LSRM 1 to other LSRM 2 and LSRM 3 (error_{12}, error_{13}) are not identical, and the maximum error between the two LSRMs (error_{23}) is falling into ± 1 mm. These results demonstrate that there exist measured disparities between the two sensors of the unit systems since the state of unit system 1 is dispatched to the two unit systems simultaneously. From graph ②, there is no communication link between unit systems 1 and 3. The state of unit system 1 is

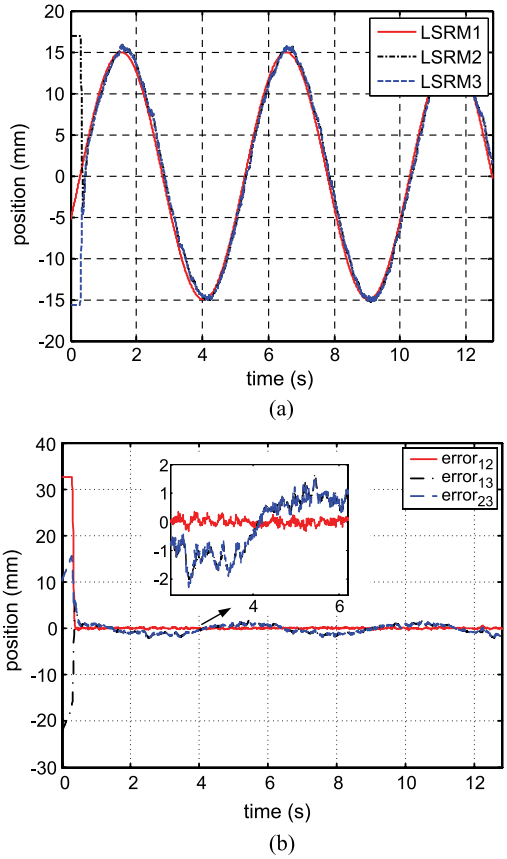

Fig. 6. Dynamic response of (a) position and (b) error of graph ②.

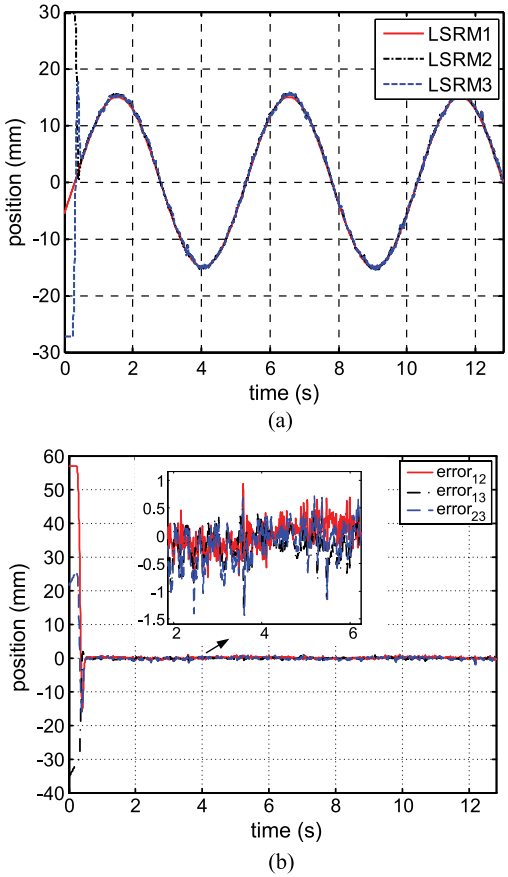

Fig. 7. Dynamic response of (a) position and (b) error of graph ③.

transmitted to unit system 2, and its state is sent to unit system 3. Unit systems 2 and 3 communicate with each other for the current status of their own. Therefore, the tracking performance between the two LSRMs is ensured, and the maximum error is falling into ± 0.4 mm. However, the graph cannot improve the tracking performance either from unit system 1 to unit system 2 or from unit system 1 to system 3. The nearly overlapped profiles of Fig. 6(a) prove the effective information flow from unit system 2 to unit system 3, so each system can track the reference signal individually with considerate dynamic errors. The topology in graph ③ guarantees the state information flow from unit system 1 to unit systems 2 and 3. Due to the unidirectional information exchange of unit systems, the dynamic error values between the two LSRMs are not as small as that from graph ②, and the maximum error falls into ± 0.9 mm. In addition, the performance of each LSRM between unit system 1 can be ensured, and the error values are smaller when compared to the results from graph ②. This is because the tracking performance from unit system 1 to unit system 2 is not influenced by system 3. In graph ④, there is no interaction between unit systems, and the tracking performance between the two LSRMs is the worst among all the topologies. In addition, the dynamic response from the reference to each unit system is not uniform since the state information of unit system 1 is dispatched to each unit system with measured errors at the same time.

For a clear illustration, the dynamic error response waveforms between LSRM 2 and LSRM 3 are drawn together as shown in Fig. 9(a). The tracking performance between the two unit systems is the best for graph ②, and the topology of ③ is second to the best. The following conclusion can be derived from the aforementioned analysis. First, it can be deluded that bidirectional interaction between the two unit systems is advantageous to the coordination performance rather than a unidirectional way. Second, the interaction between unit systems 2 and 3 is bound to improve the coordination performance, while the communication path can also affect the tracking performance from the reference to each individual system. Third, redundant communication paths are not necessary to realize a better coordination control performance. In addition, the two dispatched signals from unit system 1 to the other unit systems may lead to signal disparity and conflict to each unit system [31].

The experiment toward a bidirectional, complete graph topology is carried out. In this topology, each LSRM can communicate with the other two LSRMs, capable of receiving and dispatching information at the same time. At the time interval of (0, 2 s), the dynamic error between any two machines falls into ± 2 mm, as shown in Fig. 9(b). This is mainly because the bidirectional communication results in more accumulated measured disparities and the tracking performance between any two machines is even worse, compared to the results in graph ①. At the time of 2.4 s, the communication link between unit systems 1 and 3 is cut off. It is clear from Fig. 9(b) that the tracking performance is similar to but a little worse than the case of graph ②, due to the bidirectional link between unit systems 1 and 2. At the time of 7.5 s, the link between

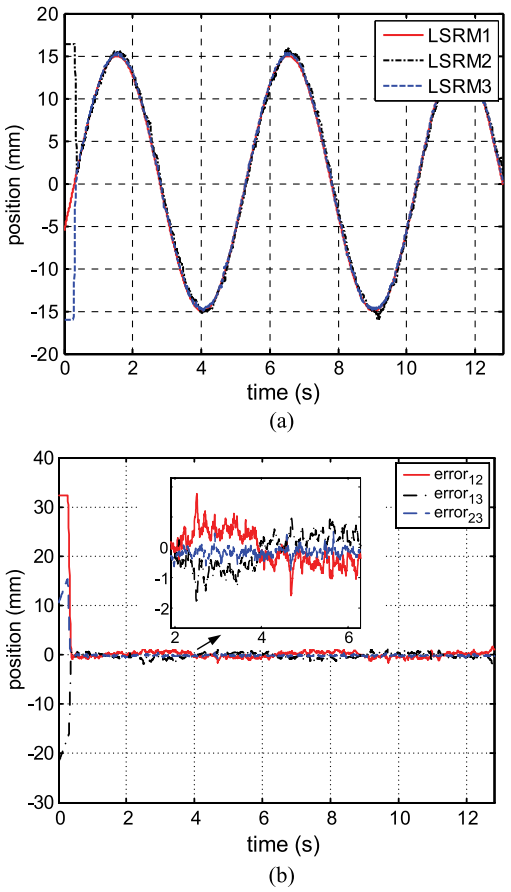

Fig. 8. Dynamic response of (a) position and (b) error of graph ④.

unit systems 2 and 3 is further broken. It can be seen that the reference signal for LSRM 3 becomes zero after some transient regulations, and LSRM 3 stops at the zero position. Fig. 9(c) shows the steady-state position response profiles as three LSRMs receive the reference signal simultaneously. It is clear that the maximum dynamic error values all fall into ±2.5 mm since all three LSRMs are strongly led by the reference independently. It can be concluded that the individual tracking and coordinated tracking are coupled. Furthermore, the individual tracking control effect with redundant reference signals acts as an external disturbance to the coordinated control effect with bidirectional communication. Fig. 9(d) shows the steady-state position response profiles under the load of 10% of mass of the moving platform imposed on unit system 2 with bidirectional communication. It is clear that the dynamic response from either two unit systems deteriorates. The relative error from unit systems 1 and 2 is worse, which may be caused by two disturbances from the reference signal and the load simultaneously.

VI. Conclusion and Discussion

The attempt for the coordinated tracking of the three direct-drive LSRM-based group motion control system is first proposed in this paper. The design and control procedure for the coordinated tracking of the three-LSRM-based unit systems is elaborated. It can be found that the graph topology possessing a bidirectional communication between unit systems guarantees an improved coordinated tracking performance; however, redundant interaction paths to the reference are actually not a necessity for further coordination performance improvement. In addition, although the tracking performance of unit system 1 influences the control performance of the entire group system,

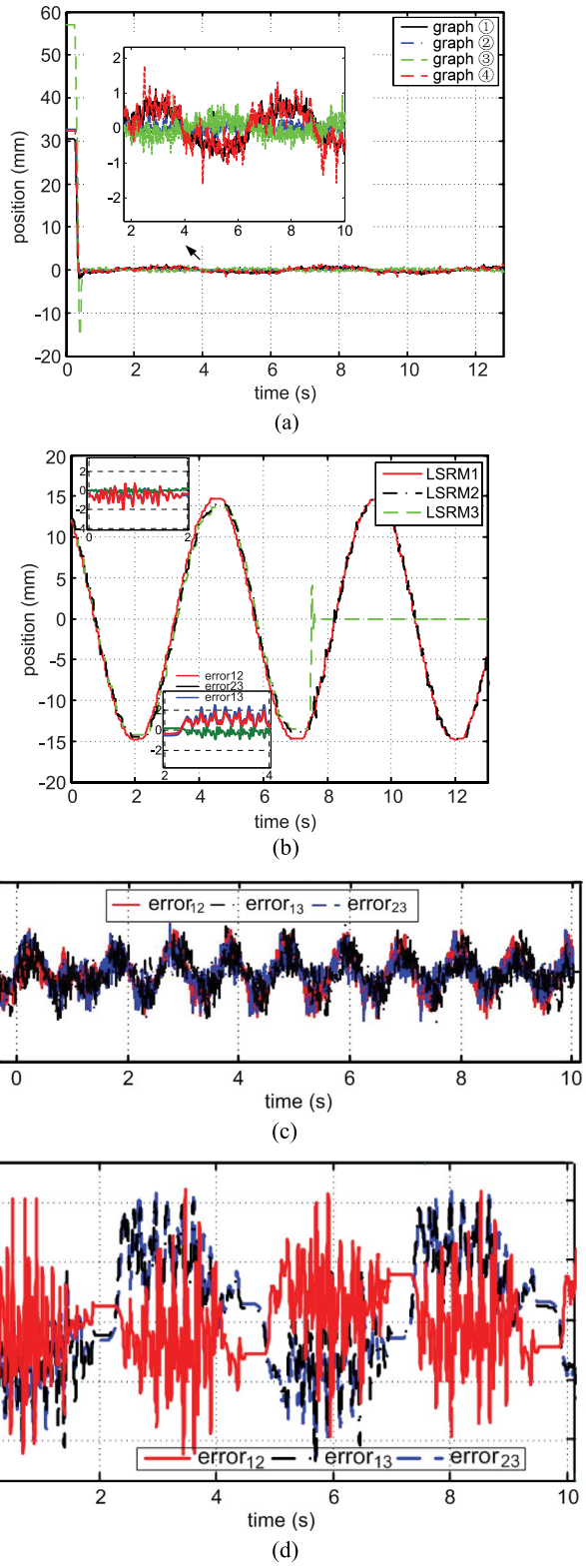

Fig. 9. Dynamic response for (a) different graphs, (b) failure simulation, (c) all unit systems receiving reference, and (d) load on unit system 2.

there are some other important factors such as package dropouts or delays, communication manners, etc., that affect the coordination performance of the group system. Furthermore, there is a lack of any closed control scheme for the entire group system globally since the state information from unit systems 2 and 3 does not provide feedback to the group system. Therefore, global closed-loop control strategies should be considered for the further improvement of the coordinated control performance.

Due to hardware limitations, the coordination control is based on three unit systems and three dSPACE control platforms. Future research will focus on the implementation of the proposed algorithm on three digital single-chip processors to further improve the group motion control performance, particularly on the annihilation of communication delays among unit systems. In addition, the detailed employment of closed and advanced group motion tracking control methods is the next work, and it is out of the scope of this paper. Furthermore, a detailed study on load influence for different unit systems will be carried out.

The ultimate goal of the implementation and study of multiple-LSRM-based group motion systems is to suggest that linear machines act as working units in manufacture and assembly lines to take advantage of the merits of linear machines. In addition, the realization of a cooperative behavior for multiple linear machines is expected to gradually replace the traditional sequenced working manner in the advanced manufacture or assembly industry.

References

[1] J. Hu, H. Xu, and Y. He, "Coordinated control of DFIG's RSC and GSC under generalized unbalanced and distorted grid voltage conditions," *IEEE Trans. Ind. Electron.*, vol. 60, no. 7, pp. 2808–2819, Jul. 2013.

[2] J. Ghommam and F. Mnif, "Coordinated path-following control for a group of underactuated surface vessels," *IEEE Trans. Ind. Electron.*, vol. 56, no. 10, pp. 3951–3963, Oct. 2009.

[3] H. Xin, Z. Qu, and A. Maknouninejad, "A self-organizing strategy for power flow control of photovoltaic generators in a distribution network," *IEEE Trans. Power Syst.*, vol. 26, no. 3, pp. 1462–1473, Aug. 2011.

[4] B. Ranjbar-Sahraei, F. Shabaninia, A. Nemati, and S. Stan, "A novel robust decentralized adaptive fuzzy control for swarm formation of multiagent systems," *IEEE Trans. Ind. Electron.*, vol. 59, no. 8, pp. 3124–3134, Aug. 2012.

[5] J. Qin, C. Yu, and H. Gao, "Coordination for linear multiagent systems with dynamic interaction topology in the leader-following framework," *IEEE Trans. Ind. Electron.*, vol. 61, no. 5, pp. 2412–2422, May 2014.

[6] P. Zeng and A. Khaligh, "A permanent-magnet linear motion driven kinetic energy harvester," *IEEE Trans. Ind. Electron.*, vol. 60, no. 12, pp. 5737–5746, Dec. 2013.

[7] J. G. Amoros and P. Andrada, "Sensitivity analysis of geometrical parameters on a double-sided linear switched reluctance motor," *IEEE Trans. Ind. Electron.*, vol. 57, no. 1, pp. 311–319, Jan. 2010.

[8] S. W. Zhao, N. C. Cheung, W. C. Gan, J. M. Yang, and Q. Zhong, "Passivity-based control of linear switched reluctance motors with robustness consideration," *IET Elect. Power Appl.*, vol. 2, no. 3, pp. 164–171, May 2008.

[9] J. F. Pan, Y. Zou, and G. Cao, "Adaptive controller for the double-sided linear switched reluctance motor based on the nonlinear inductance modeling," *IET Elect. Power Appl.*, vol. 7, no. 1, pp. 1–15, Jan. 2013.

[10] J. Lin *et al.*, "Active suspension system based on linear switched reluctance actuator and control schemes," *IEEE Trans. Veh. Technol.*, vol. 62, no. 2, pp. 562–572, Feb. 2013.

[11] C. W. Reynolds, "Flocks, herds and schools: A distributed behavioral model," *ACM SIGGRAPH Comput. Graph*, vol. 21, no. 4, pp. 25–34, Jul. 1987.

[12] T. Vicsek and A. Zafeiris, "Collective motion," *Phys. Rep.*, vol. 517, pp. 71–140, 2012.

[13] I. D. Couzin, J. Krause, and N. R. Franks, "Effective leadership and decision-making in animal groups on the move," *Nature*, vol. 433, no. 7025, pp. 513–516, Mar. 2005.

[14] W. Ren and R. W. Beard, *Distributed Consensus in Multi-Vehicle Cooperative Control*. London, U.K.: Springer-Verlag, 2008, pp. 121–123.

[15] Z. Qu, J. Wang, and R. A. Hull, "Cooperative control of dynamical systems with application to autonomous vehicles," *IEEE Trans. Autom. Control*, vol. 53, no. 4, pp. 894–911, May 2008.

[16] I. Bayezit and B. Fidan, "Distributed cohesive motion control of flight vehicle formations," *IEEE Trans. Ind. Electron.*, vol. 60, no. 12, pp. 5763–5772, Dec. 2013.

[17] R. Olfati-Saber, J. A. Fax, and R. M. Murray, "Consensus and cooperation in networked multi-agent systems," *Proc. IEEE*, vol. 95, no. 1, pp. 215–233, Jan. 2007.

[18] A. Zou, "Distributed attitude synchronization and tracking control for multiple rigid bodies," *IEEE Trans. Control Syst. Technol.*, vol. 22, no. 2, pp. 478–490, Mar. 2014.

[19] A. Zou, "Finite-time output feedback attitude tracking control for rigid spacecraft," *IEEE Trans. Control Syst. Technol.*, vol. 22, no. 1, pp. 338–345, Jan. 2014.

[20] P. Massioni, T. Keviczky, E. Gill, and M. Verhaegen, "A decomposition-based approach to linear time-periodic distributed control of satellite formations," *IEEE Trans. Control Syst. Technol.*, vol. 19, no. 3, pp. 481–492, May 2011.

[21] H. Song, L. Yu, and W. Zhang, "Distributed consensus-based Kalman filtering in sensor networks with quantised communications and random sensor failures," *IET Signal Process.*, vol. 8, no. 2, pp. 107–118, Apr. 2014.

[22] A. Guillet, R. Lenain, B. Thuilot, and P. Martinet, "Adaptable robot formation control: Adaptive and predictive formation control of autonomous vehicles," *IEEE Robot. Autom. Mag.*, vol. 21, no. 1, pp. 28–39, Mar. 2014.

[23] J. F. Pan, Y. Zou, and G. Cao, "An asymmetric linear switched reluctance motor," *IEEE Trans. Energy Conversion*, vol. 28, no. 2, pp. 444–451, Jun. 2013.

[24] H. Zhang, G. Feng, H. Yan, and Q. Chen, "Observer-based output feedback event-triggered control for consensus of multi-agent systems," *IEEE Trans. Ind. Electron.*, vol. 61, no. 9, pp. 4885–4894, Sep. 2014.

[25] Z. Qu, *Cooperative Control of Dynamical Systems*. Berlin, Germany: Springer-Verlag, 2009, pp. 78–79.

[26] Z. Li, Z. Duan, G. Chen, and L. Huang, "Consensus of multiagent systems and synchronization of complex networks: A unified viewpoint," *IEEE Trans. Circuits Syst. I, Reg. Papers*, vol. 57, no. 1, pp. 213–224, Jan. 2010.

[27] J. Pan, N. C. Cheung, and J. Yang, "High-precision position control of a novel planar switched reluctance motor," *IEEE Trans. Ind. Electron.*, vol. 52, no. 6, pp. 1644–1652, Dec. 2005.

[28] J. F. Pan and N. C. Cheung, "An adaptive controller for the novel planar switched reluctance motor," *IET Elect. Power Appl.*, vol. 5, no. 9, pp. 677–683, Nov. 2011.

[29] Z. Meng, W. Ren, Y. Cao, and Z. You, "Leaderless and leader-following consensus with communication and input delays under a directed network topology," *IEEE Trans. Syst., Man, Cybern. B, Cybern.*, vol. 41, no. 1, pp. 75–88, Feb. 2011.

[30] H. Zhang, F. L. Lewis, and Z. Qu, "Lyapunov, adaptive, and optimal design techniques for cooperative systems on directed communication graphs," *IEEE Trans. Ind. Electron.*, vol. 59, no. 7, pp. 3026–3041, Jul. 2012.

[31] Y. Shi, J. Huang, and B. Yu, "Robust tracking control of networked control systems: Application to a networked dc motor," *IEEE Trans. Ind. Electron.*, vol. 60, no. 12, pp. 5864–5874, Dec. 2013.

Bo Zhang (M'15) received the Ph.D. degree from Northwestern Polytechnical University, Xi'an, China, in 2013.

He is currently a Lecturer with the College of Mechatronics and Control Engineering, Shenzhen University, Shenzhen, China. His main research interests are the modeling and control of group motion systems.

Jianping Yuan received the B.S. and Ph.D. degrees from Northwestern Polytechnical University, Xi'an, China, in 1982 and 1985, respectively.

He is currently a Professor in the School of Astronautics, Northwestern Polytechnical University. His research interests are spacecraft flight dynamics and control, and space robotics cluster technology.

Li Qiu received the B.S. degree in control engineering from Jinan University, Jinan, China, in 2003, and the M.E. and Ph.D degrees in control theory and control engineering from South China University of Technology, Guangzhou, China, in 2006 and 2011, respectively.

She is a Lecturer in the College of Mechatronics and Control Engineering of Shenzhen University, Shenzhen, China. Her current research interests include networked control systems, Markovian jump linear systems, analysis and synthesis of time-delay systems, uncertain systems, and robust control.

Norbert Cheung (SM'05) received the M.Sc. degree from the University of Hong Kong, Hong Kong, in 1987 and the Ph.D. degree from the University of New South Wales, Sydney, Australia, in 1995.

He is currently an Associate Professor in the Department of Electrical Engineering, Hong Kong Polytechnic University, Hong Kong. His research interests are motion control, actuator design, and power electronic drives.

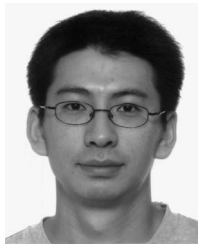

J. F. Pan (M'15) received the Ph.D. degree from the Department of Electrical Engineering, Hong Kong Polytechnic University, Hong Kong, in 2006.

He is currently a Professor with the College of Mechatronics and Control Engineering, Shenzhen University, Shenzhen, China. His main research interests are the design and control of switched reluctance motors and generators.